Philosophical Magazine Letters

ISSN: 0950-0839 (Print) 1362-3036 (Online) Journal homepage: https://www.tandfonline.com/loi/tphl20

Dynamic precipitation of Al–Zn alloy during rolling and accumulative roll bonding

C.Y. Liu, L. Yu, M.Z. Ma, R.P. Liu & Z.Y. Ma

To cite this article: C.Y. Liu, L. Yu, M.Z. Ma, R.P. Liu & Z.Y. Ma (2015) Dynamic precipitation of Al–Zn alloy during rolling and accumulative roll bonding, Philosophical Magazine Letters, 95:11, 539-546, DOI: 10.1080/09500839.2015.1119322

To link to this article: https://doi.org/10.1080/09500839.2015.1119322

Philosophical Magazine Letters, 2015
Vol. 95, No. 11, 539–546, http://dx.doi.org/10.1080/09500839.2015.1119322

Taylor & Francis
Taylor & Francis Group

Dynamic precipitation of Al–Zn alloy during rolling and accumulative roll bonding

C.Y. Liu[a,b], L. Yu[a], M.Z. Ma[b], R.P. Liu[b]* and Z.Y. Ma[c]*

[a]*Key Laboratory of New Processing Technology for Nonferrous Metal & Materials, Ministry of Education, Guilin University of Technology, Guilin 541004, China;* [b]*State Key Laboratory of Metastable Materials Science and Technology, Yanshan University, Qinhuangdao 066004, China;* [c]*Shenyang National Laboratory for Materials Science, Institute of Metal Research, Chinese Academy of Sciences, 72 Wenhua Road, Shenyang 110016, China*

(*Received 8 July 2015; accepted 7 November 2015*)

In this study, cold rolling was performed on a binary Al–20 wt%Zn alloy and dynamic precipitation identified for the first time in Al alloys under cold rolling. Zn clusters formed after application of 0.6 strain, and the Zn phase precipitated upon further increasing strain. Both grain refinement and rolling-induced defects are considered to promote Zn precipitation. The hardness of Al–Zn alloy initially increased with strain up to a strain of 2.9 and then decreased with increasing rolling strain. Dynamic precipitation greatly affects the strengthening mechanism of the rolled Al–Zn alloy under various strains.

Keywords: Al–Zn alloy; cold rolling; dynamic precipitation; hardening

1. Introduction

Severe plastic deformation (SPD) is attracting significant research interest because of its effectiveness in fabricating nanocrystalline and ultrafine-grained (UFG) Al alloys. Recently, dynamic precipitation has been demonstrated during SPD, which it was noted greatly affects the properties of Al alloys. In particular, dynamic precipitation can improve the superplastic property of UFG Al alloys by pinning the grain boundaries (GBs) during hot deformation [1], enhance the electrical conductivity of high-strength UFG Al alloys by decomposing the solid solution [2] and improve the room temperature (RT) ductility of UFG Al alloys by promoting GB sliding [3]. Interestingly, dynamic precipitation can either harden certain Al alloys by means of nano-sized particles [4], or soften others by decomposing the solid solution [5–8].

According to current strengthening theories, there are two competing effects of deformation on the hardness of Al alloys: (i) hardening by grain refinement, increase of dislocations and presence of nano-sized precipitates; and (ii) softening by the decomposition of supersaturated solid solution, coarsening of precipitates, coarsening of Al grains after completion of dynamic recrystallization (DRX) and annihilation of dislocations. Dynamic precipitation can increase precipitation strengthening and simultaneously affect other strengthening mechanisms. In particular, precipitation can lead to the decrease in solid solution strengthening, enhancement of matrix grain refinement with

*Corresponding authors. Email: riping@ysu.edu.cn (R.P. Liu); zyma@imr.ac.cn (Z.Y. Ma)

consequent increase of grain-boundary strengthening [9,10] and increase in dislocation storage capability with resulting enhancement of dislocation strengthening [11]. Thus, dynamic precipitation plays an important role in the microstructure and mechanical properties of UFG Al alloys fabricated through SPD.

Dynamic precipitation has been investigated under high-pressure torsion (HPT) [2,3,5–10,12,13] and equal channel angular pressing (ECAP) [14] for many years. It was reported that the static and dynamic precipitations as well as dissolution of precipitates occur at the same time during HPT and ECAP owing to the long deformation time [14]. This indicates that the effect of deformation on the segregation and precipitation in Al alloys is very complicated [10,15,16].

Low-temperature rolling, including accumulative roll bonding (ARB) [17], is another important deformation process. Compared with HPT and ECAP, rolling uses a much higher deformation speed. Thus, the load time during rolling can be neglected and the effect of strain on the dynamic precipitation may be more easily clarified. However, previous research showed that the strength–structure relationship of as-rolled Al alloys is consistent well with the Hall–Petch relationship [18,19]. This means that the grain refinement plays a dominant role in the microstructural changes in Al alloys during rolling and the decomposition of solid solution during rolling are insufficiently sensitive to strain. Therefore, more research is needed to elucidate dynamic precipitation behaviour of Al alloys during rolling.

In the present study, a supersaturated solid solution of Al–Zn, which decomposed easily during HPT (within one anvil revolution) [5–8], was used as the raw material to investigate the dynamic precipitation behaviour of Al alloys during rolling. The interaction of solute atoms with crystalline defects, such as vacancies, dislocations and GBs, during rolling was analysed. Vickers hardness was correlated to the microstructures through the strength–structure relationship, which is discussed based on the operation of different strengthening mechanisms.

2. Experimental methods

Al–20 wt% Zn alloy was prepared by melting high-purity components in vacuum. The castings were cut into samples with dimensions of 16 × 80 × 200 mm and were solution treated at 550 °C for 3 h and quenched in water (designated as WQ sample). Samples were then rolled from 16 to 0.5 mm in 10 passes (about 1.5 mm thickness reduction per pass and about 97% thickness reduction in total) at RT. The rolling speed was 0.5 m/s. Afterwards, ARB was used to obtain a larger deformation degree. The 0.5 mm-thick rolled sheets, as the starting material for ARB, were cut into two halves after surface treatment, and then stacked together and rolled to 50% reduction at RT. This cycle was repeated for up to 10 cycles. According to the literature [20], the equivalent plastic strain ε of the ARB sample can be expressed as follows:

$$\varepsilon = \left\{ \frac{2}{\sqrt{3}} \ln\left(\frac{t}{t_0}\right) \right\} + 0.8n \tag{1}$$

where t_0 is the initial thickness of the sample, t is the thickness of the rolled sample in the rolling process and n is the number of cycles for ARB. The largest ε of the as-deformed sample can reach up to ~12.1 (10 cycles of ARB after 97% rolling reduction).

The phase structures of the Al–Zn samples were determined by X-ray diffraction (XRD). The microstructures were examined using electron backscattered diffraction (EBSD) and transmission electron microscopy (TEM). Hardness measurement was conducted using a Vickers microhardness tester (using 9.8 N load for 15 s).

3. Results and discussion

Figure 1 shows the continuously increasing intensity of Zn XRD peaks with increasing plastic strain, which signifies the precipitation of Zn phase during rolling. The atomic radius of Zn (0.153 nm) is smaller than that of Al (0.182 nm). As the Al–Zn solid solution decomposes, the lattice parameter of the Al matrix increases and the Al peaks shift towards the low-angle orientation, as shown by the insert in Figure 1.

Figure 2 shows that the microstructure of WQ Al–20% Zn alloy was characterized by large-sized Al grains (larger than 200 μm as shown in Figure 2a), an absence of precipitates, a low density of dislocations and well-defined GBs (Figure 2b).

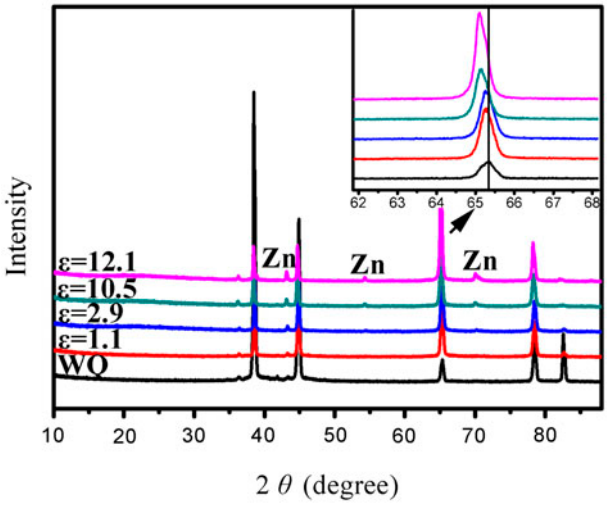

Figure 1. XRD of WQ and rolled Al–20% Zn samples after different rolling strains.

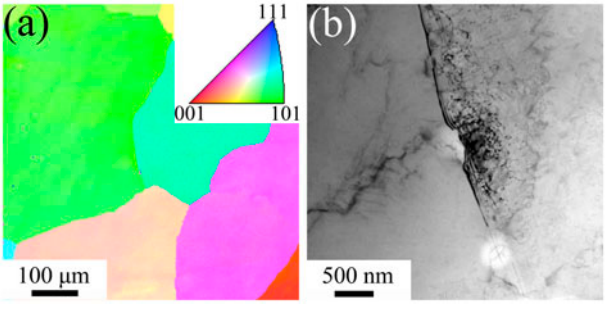

Figure 2. Microstructure of WQ Al–20% Zn alloy: (a) EBSD and (b) TEM image.

Figure 3 shows the microstructure of rolled Al–20% Zn alloy with different strains. RT rolling under a small degree of deformation (0.6) induced the formation of dispersoids with sizes below 5 nm as shown in Figure 3a. An inverse fast Fourier transformation (IFFT) of the high-resolution transmission electron microscope (HRTEM) image in the framed area in Figure 3a is shown in Figure 3b. As can be seen, there is no mismatch of the lattice planes between dispersoid and Al matrix, suggesting coherency between the Al matrix and dispersoid. So, the dispersoids are the Zn atom-rich region (clusters) and also form a solid solution in the Al lattice. A large number of dislocations were observed near the dispersoid–matrix interface (*T* in Figure 3b), and this means that

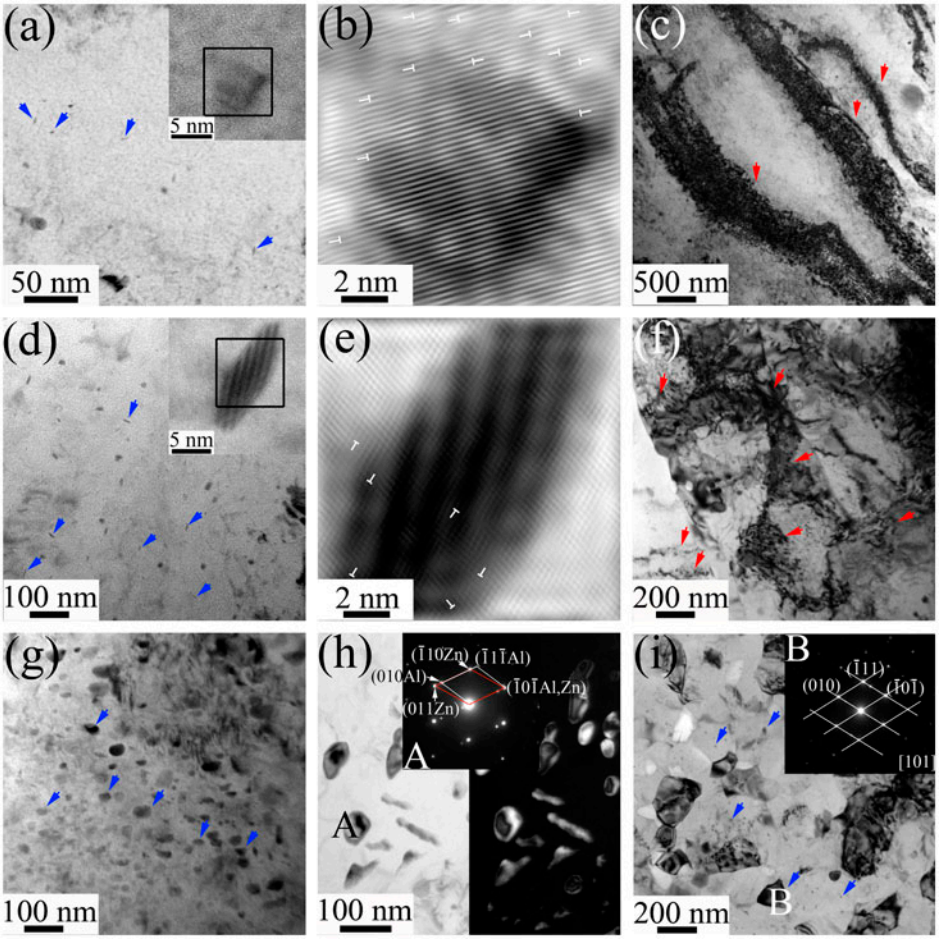

Figure 3. TEM images of rolled Al–20% Zn alloy with strains of (a) and (b) 0.6, (c), (d) and (e) 1.1, (f) and (g) 2.9, (h) 4.1 and (i) 12.1. The inset in (a) and (d) are HRTEM images of Al–20% Zn alloy with strains of 0.6 and 1.1, respectively. (b) and (e) are the IFFT images of the frames inserted in (a) and (d), respectively. The inset in (h) and (i) are SAD using areas A and B, respectively. Red arrows denote dislocation tangles/walls, blue arrows denote the dispersoids, and '*T*' denotes dislocation cores. All of the images were taken from RD–TD planes.

cold rolling with a small strain induced a large number of crystalline defects around the dispersoids.

After application of 1.1 rolling strain, a high density of dislocations was observed in the Al–Zn alloy as tangles and walls, and rod-like dispersoids with sizes of approximately 15 nm were obtained (Figure 3c and d). Figure 3e is an IFFT of the HRTEM image in the framed area of Figure 3d. Periodic moiré fringes appeared in the dispersoid, suggesting that the Zn phase precipitated from Al lattice. A large number of dislocations were observed in both Al matrix and dispersoid.

On further increasing the strain to 2.9, as shown in Figure 3f and g, elongated Al grains were obtained, and a large number of dislocations were observed to fix at the subgrain boundaries (SBs). Furthermore, the dispersoids coarsened and changed to an equiaxed shape.

Figure 3h shows bright-field (BF) images, dark-field (DF) images and selected area diffraction (SAD) pattern of rolled Al–20% Zn alloy with 4.1 strain. BF image shows that the dispersoids further coarsened. The SAD spots show that both Zn and Al phase were observed in the selected area 'A'. DF image excited using the {1 1 0} reflection of Zn phase further confirmed that this phase consists of Zn particles.

Figure 3i shows the microstructure of the Al–Zn alloy after SPD with an equivalent strain of 12.1. The grain size of Al matrix was reduced to 150 nm (about 10^3 times smaller than that of WQ sample), with considerably low dislocation density. Particle 'B' represents the Zn phase, which was identified based on its SAD pattern. Two types of Zn phases were present in this sample. Type 1 measured 50–150 nm in size and was located at the triple junctions of the Al grains, whereas type 2 measured below 15 nm in size and was found within the Al grains.

Sauvage et al. [21] found that Mg atoms could be dragged by deformation-induced vacancies during HPT. In contrast, Zn atoms exhibited greater instability in the Al matrix under deformation conditions [6]. Therefore, rolling-induced vacancies can cause more Zn atoms to move and consequently Zn clusters form more easily (Figure 3a). Larger defects, such as the dislocations tangles/walls demonstrated in the TEM image, also formed during rolling. These defects may obstruct the movement of vacancies, arrest Zn cluster formation and subsequently cause the appearance of nano-sized Zn particles within the Al grains. So, rod-like precipitates, which are similar to the shape of the defects, are observed (Figure 3d).

The schematic illustration of early stage dynamic precipitation in the Al–Zn alloy is shown in Figure 4a. The rod-like phase was not obtained in the as-HPT Al–Zn alloys [5–8], probably because the duration of deformation in HPT was much longer than that in rolling and the rod-like dislocations readily tangle and evolve to dislocation cells.

A large number of dislocations were found near the nano-sized precipitate/matrix interfaces after rolling as shown in Figure 3b and e (the *T* symbol). The dislocations also arrest Zn cluster formation during rolling and then cause the Zn phase to coarsen and a change of shape to equiaxed form (a schematic illustration is shown in Figure 4b).

With further rolling, elongated grains and a large number of SBs formed. Before completion of DRX, the grain boundaries are often designated as 'non-equilibrium GBs' because those GBs contain a large number of dislocations (Figure 3f). The non-equilibrium GBs act as dislocation sinks; most of the dislocations are absorbed along boundaries where they dynamically recover. The Zn clusters and nano-sized precipitates were strongly coupled to dislocations, and the mobile dislocations drag the Zn clusters

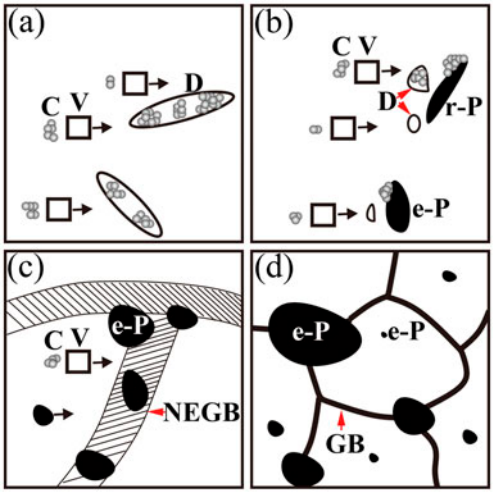

Figure 4. Schematic illustration of dynamic precipitation of Zn phases in Al–Zn alloy during rolling. The strain increased gradually from (a) to (d). 'C' represents clusters, 'V' represents vacancies, 'D' represents dislocations, 'r-P' represents particles with rod-like shape, 'e-P' represents particles with equiaxed shape, 'NEGB' represents non-equilibrium grain boundary, 'GB' represents grain boundary.

to precipitate during rolling. Thus, the Zn particles tended to gather in the SBs. The SBs continuously shift to the high-angle grain boundaries during SPD (ARB stage); hence the coarsened Zn particles tended to situate at the triple junctions of the Al grains. The Al matrix grain size was reduced to UFG after the completion of DRX. Newly formed GBs were also heavily enriched with Zn atoms. Therefore, diffusion of Zn towards larger growing precipitates (50–150 nm) occurred at the GBs rather than in the bulk of the material. Some of the newly precipitated Zn phases with sizes below 15 nm lacked sufficient time to diffuse into the GBs and consequently presented within the Al grains after rolling. The schematic of dynamic precipitation during SPD is illustrated in Figure 4c and d.

It is worth mentioning that the rolling speed is low and the thickness of samples is 0.5 mm in this study (they were often 1 mm in the previous ARB studies [17,20,22]), therefore the temperature rise and cooling rate of samples during rolling in this study are lower and faster than those in previous ARB studies. So, the effect of adiabatic heating caused by deformation on the kinetics of precipitation can be ignored.

Mazilkin et al. [6] demonstrated that the hardness of Al–Zn alloys decreases substantially during HPT. The softening effect caused by the decomposition of supersaturated solid solution is more pronounced than the hardening effects contributed by the increase of dislocations, refinement of grains and presence of precipitates. In the present study, the trend in the change of hardness during rolling differs from that during HPT, as shown in Fig. 5. The hardness of the Al–Zn alloy initially increased with increasing rolling strain, and the peak hardness of 119 HV appeared at an equivalent plastic strain of 2.9. Compared with the microstructure of the as-HPT sample, that of the Al–Zn alloy showed finer precipitates, a high density of dislocations and higher solubility (13% test by EDS) after the application of 2.9 rolling strain. Overall, precipitation strengthening

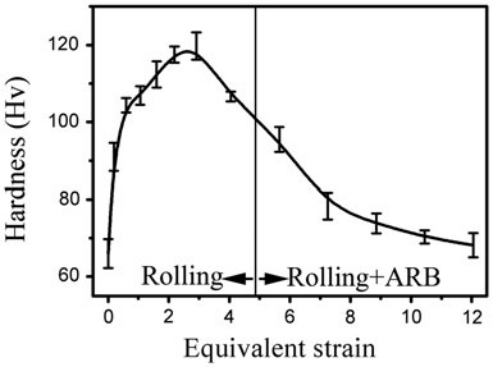

Figure 5. Variation of Vickers hardness with equivalent strain during rolling for Al–20% Zn alloy.

by nano-sized precipitates, work hardening by dislocations and solid solution strengthening by lattice distortion are the main strengthening mechanisms in this sample.

The hardness of the Al–Zn alloy continuously reduced with increasing strain from 2.9 to 12.1. In this process, the decrease in work hardening due to the annihilation of dislocations, precipitation strengthening caused by to the coarsening of precipitates and solid solution strengthening due to the decomposition of solid solution is more pronounced than the increase in boundary hardening arising from continuous grain refinement. The net effect results in the softening of Al–Zn alloy during rolling.

The hardness of the present UFG Al–Zn alloy is greater than that of UFG pure Al produced by rolling in our previous work [22]. Compared with UFG pure Al, the UFG Al–Zn alloys exhibited finer grain sizes because of the pinning effect of Zn particles on GBs during rolling. Furthermore, enhancement of boundary hardening occurred in the UFG Al–Zn alloy.

4. Conclusions

In summary, dynamic precipitation has been demonstrated in Al–Zn alloy during rolling. The evolution process of dynamic precipitation was identified: (1) Zn cluster formation due to vacancy drag, (2) arrest in dislocations and (3) formation of rod-like phase. With increasing rolling strain further, the precipitates coarsened and changed to an equiaxed shape and finally were fixed at the triple junctions of the Al grains. The hardness of Al–Zn alloy increased with increasing strain, up to a peak value of 119 HV at a strain of 2.9 and then decreased with further strain increase. Dynamic precipitation greatly affects the strengthening mechanism of the rolled Al–Zn alloys.

Acknowledgement

The authors would like to thank Pengfei Yu for the TEM observations.

Disclosure statement

No potential conflict of interest was reported by the authors.

Funding

This work was funded by the National Basic Research Program of China [grant number 2013CB733000]; Guangxi Natural Science Foundation [grant number 2015GXNSFBA139238]; Guangxi 'Bagui' Teams for Innovation and Research.

References

[1] Z.Y. Ma, F.C. Liu and R.S. Mishra, Acta Mater. 58 (2010) p.4693.
[2] R.Z. Valiev, M.Y. Murashkina and I. Sabirov, Scr. Mater. 76 (2014) p.13.
[3] R.Z. Valiev, M.Y. Murashkin, A. Kilmametov, B. Straumal, N.Q. Chinh and T.G. Langdon, J. Mater. Sci. 45 (2010) p.4718.
[4] U.G. Kang, H.J. Lee and W.J. Nam, J. Mater. Sci. 47 (2012) p.7883.
[5] M. Borodachenkova, F. Barlat, W. Wen, A. Bastos and J.J. Grácio, Int. J. Plasticity 68 (2015) p.150.
[6] A.A. Mazilkin, B.B. Straumal, E. Rabkin, B. Baretzky, S. Enders, S.G. Protasova, O.A. Kogtenkova and R.Z. Valiev, Acta Mater. 54 (2006) p.3933.
[7] B. Straumal, R. Valiev, O. Kogtenkova, P. Zieba, T. Czeppe, E. Bielanska and M. Faryna, Acta Mater. 56 (2008) p.6123.
[8] B. Straumal, B. Baretzky, A. Mazilkin, F. Phillipp, O.A. Kogtenkova, M.N. Volkov and R.Z. Valiev, Acta Mater. 52 (2004) p.4469.
[9] K. Tugcu, G. Sha, X.Z. Liao, P. Trimby, J.H. Xia, M.Y. Murashkin, Y. Xie, R.Z. Valiev and S.P. Ringer, Mater. Sci. Eng. A 552 (2012) p.415.
[10] G. Sha, K. Tugcu, X.Z. Liao, P.W. Trimby, M.Y. Murashkin, R.Z. Valiev and S.P. Ringer, Acta Mater. 63 (2014) p.169.
[11] Y.H. Zhao, X.Z. Liao, S. Cheng, E. Ma and Y.T. Zhu, Adv. Mater. 18 (2006) p.2280.
[12] A. Alhamidi, K. Edalati, Z. Horita, S. Hirosawa, K. Matsuda and D. Terada, Mater. Sci. Eng. A 610 (2014) p.17.
[13] G. Nurislamova, X. Sauvage, M. Murashkin, R. Islamgaliev and R. Valiev, Philos. Mag. Lett. 88 (2008) p.459.
[14] I. Gutierrez-Urrutia, M.A. Muñoz-Morris and D.G. Morris, Mater. Sci. Eng. A 394 (2005) p.399.
[15] G. Sha, L. Yao, X.Z. Liao, S.P. Ringer, Z.C. Duan and T.G. Langdon, Ultramicroscopy 111 (2011) p.500.
[16] P.V. Liddicoat, X.Z. Liao, Y.H. Zhao, Y.T. Zhu, M.Y. Murashkin, E.J. Lavernia, R.Z. Valiev and S.P. Ringer, Nat. Commun. 1 (2010) p.63.
[17] Y. Saito, N. Tsuji, H. Utsunomiya, T. Sakai and R.G. Hong, Scr. Mater. 39 (1998) p.1221.
[18] H. Jin and D.J. Lloyd, Scr. Mater. 50 (2004) p.1319.
[19] W.J. Kim, J.Y. Wang, S.O. Choi, H.J. Choi and H.T. Sohn, Mater. Sci. Eng. A 520 (2009) p.23.
[20] Y. Saito, H. Utsunomiya, N. Tsuji and T. Sakai, Acta Mater. 47 (1999) p.579.
[21] X. Sauvage, N. Enikeev, R. Valiev, Y. Nasedkina and M. Murashkin, Acta Mater. 72 (2014) p.125.
[22] C.Y. Liu, B. Zhang, P.F. Yu, R. Jing, M.Z. Ma and R.P. Liu, Mater. Sci. Eng. A 580 (2013) p.36.